RSC Advances

PAPER

View Article Online
View Journal | View Issue

Cite this: *RSC Adv.*, 2020, **10**, 14360

High iodine adsorption performances under off-gas conditions by bismuth-modified ZnAl-LDH layered double hydroxide

Trinh Dinh Dinh, [ab] Dongxiang Zhang*[a] and Vu Ngoc Tuan[c]

The effective adsorption of radioactive iodine is greatly desirable, but is still a significant challenge. In this manuscript, we report the synthesis of a bismuth-modified zinc aluminium layered double hydroxide (BiZnAl-LDH) *via* a co-precipitation method for the highly efficient absorption of iodine. Based on the robust chemical attraction between Bi and I_2, BiZnAl-LDH exhibited highly effective iodine capture. Furthermore, to evaluate BiZnAl-LDH as an effective sorbent, it was characterized *via* X-ray powder diffraction (XRD), scanning electron microscopy-energy dispersion spectroscopy (SEM-EDS), and Fourier-transform infrared spectroscopy (FITR). In addition, to determine the morphology and iodine adsorption properties of BiZnAl-LDH, several studies were conducted. Through experiments, its elemental composition and vibration before and after iodine adsorption were analyzed *via* EDS and X-ray photoelectron spectroscopy (XPS). During the capture process, I_2 is reduced to I^- by the intercalated Bi^{3+} *via* chemical adsorption, and the maximum adsorption capacity of BiZnAl-LDH for iodine reached up to 433 mg g^{-1}, which had a surface area, average pore diameter, and pore volume of 36.259 m^2 g^{-1}, 2.374 nm, and 0.128 m^3 g^{-1}, respectively. Compared with several previous sorbents for iodine adsorption, BiZnAl-LDH exhibited an iodine adsorption of approximately two times that of the commercial Ag-exchange zeolite X, and furthermore BiZnAl-LDH is cost-effective. Thus, the substantial iodine capture by BiZnAl-LDH indicates that it is a capable sorbent for the effective elimination of radioactive iodine from reprocessing plant emissions.

Received 17th January 2020
Accepted 20th March 2020

DOI: 10.1039/d0ra00501k

rsc.li/rsc-advances

1. Introduction

With the speedy development of nuclear energy, the safe removal of radioactive waste generated in the nuclear fuel cycle has become an issue of great concern to society.[1,2] Isotopes of radioactive iodine are one type of hazardous radionuclide produced through the nuclear fission of ^{235}U.[3,4]

Among the existing isotopes of iodine, ^{127}I is the most common and stable one. Also, ^{127}I can be commonly found in foodstuff, where it is used as an additional nutritional supplement (*e.g.* iodized salt). Furthermore, considering its application potential as an antimicrobial agent, it is also used for immediate water sterilization in emergency or critical cases.[5] In addition, to reduce the chances of the physical uptake of rarer radioactive isotopes from the environment, ^{127}I can be used in large doses. Nevertheless, studies reveal[6,7] that this approach is dangerous in the long term.

As a result of its application in nuclear industrial energy, the ^{131}I isotope has received considerable attention in recent years. ^{131}I has found successful applications in the medical industry, where it has become a widely used product for medical imaging in nuclear medicine and radiation therapy. As a byproduct of the nuclear energy industry, where it is produced as a result of the fission of uranium, its acquisition, and application in countries that do not use atomic energy is limited. Based on the comparatively short radioactive half-life of ^{131}I, which is 8 days, it is considered a major health hazard. In some cases, it has been found where a nuclear accident occurred within the first week.[8] On the other hand, the ^{129}I isotope has a long-term radioactive half-life of over a few million years and is substantially less dense than other isotopes. However, ^{129}I is of significant interest in several fields and disciplines such as geological and environmental sciences. To quantitatively measure the human impact on the atmosphere, ^{129}I can be used as a significant unit measure, in particular the effect of the nuclear blast during nuclear bomb testing on the new atmosphere.[9]

There is a vast body of research primarily focused on the radioactive waste products from the exhaust stream. Indeed, there are well-known wet processes designed to trap radioactive iodine. For example, mercury and alkaline scrubbing have proven to have highly effective removal capacities, anion

[a]*School of Chemistry and Chemical Engineering, Beijing Institute of Technology, Beijing, 102488, China. E-mail: boris@bit.edu.cn; Tel: +86 13366112230*
[b]*Vilas 849, Quality Testing Lab, Center for Research and Development Science Technology Tien Nong, Thanh Hoa, 442410, Vietnam*
[c]*Faculty of Electric-Electronic Engineering, Nam Dinh University of Technology Education, Nam Dinh, 420000, Vietnam*

exchange resins,[10,11] zeolite-based materials,[12,13] Ag-based material,[14,15] porous metal–organic frameworks (MOFs),[16–19] Cu-based materials,[20,21] and in the case of adsorbents for the adsorption of radioactive I^-, activated carbon.[22] In addition, several research groups have studied the depletion potential of different iodine species containing I^- and IO_3^- from aqueous solutions of layered double hydroxides (LDHs).[8,9]

LDHs are known as anionic clays materials or hydrotalcite-like compounds, which are coating-stratified clay metals based on a similar structure to the brucite $Mg(OH)_2$. LDHs also present a layered structure that carries a net positive charge. Their exchangeable anions are balanced by the positive charge constituents of the alternating cation layers in the alternating regions of LDHs. The common formula of LDHs is characterized by $M^{2+}_{1-y}M^{3+}_y(OH)^{y+}_2(A^{n-})_{y/n}\cdot mH_2O$ where the divalent metal M^{2+} is Ni^{2+}, Cu^{2+}, Mg^{2+} and Zn^{2+} cation, the trivalent metal M^{3+} is Ti^{3+}, Al^{3+}, Bi^{3+} and Fe^{3+} cation, usually chloride, nitrate or carbonate is the exchangeable anion and y is usually $0.2 < y < 0.33$.[23,24] The structure and composition of LDH compounds have been the focus of considerable research. In addition, the recent work by Mills *et al.* based on hydrotalcite LDHs exhibited an interesting property in terms of composition and nomenclature called the reform effect (or remembrance).[25] Basic metal adsorbents have been effectively applied in iodine adsorption. Moreover, Nenoff and colleagues conducted substantial work aimed at advancing layered hydrotalcite-like oxides-I-Bi as waste forms for iodine precipitation. As a result, it was found that the iodine phase composition in oxides-I-Bi was determined according to the Bi : I ratio,[26,27] and the compounds containing bismuth showed several important advantages such as the ability to react with iodine and iodide capture capacity, and Bi_2O_3 was also comprehensively investigated for iodine immobilization adsorption.[28–30]

It was reported that the surface modification of layered double hydroxide electrodes with an additive, such as Bi, can enhance the chemical properties of the active materials.[31–33] Also, layered double hydroxide materials have been investigated as additives due their effect on the environment. The main additives to Al include bismuth and other non-metallic elements, including other bismuth compounds and Bi_2O_3. These bismuth compounds can prove the linkage efficiency between Bi and the zinc metal matrix.[34] Moreover, an Al–Bi mixed system can allow Bi-phase stabilization and overcome some of the limitations of Al.

We investigated bismuth for the capture of iodine gas. The reactions between iodine and bismuth demonstrate the characteristic properties of the gas–solid reaction in the iodine adsorption process. Table 1 clearly shows the highly exothermic nature of this reaction and that the iodine adsorption capacity of Bi is better than that of silver and Bi_2O_3.

High iodine adsorption efficiency is highly desirable, but there are still major challenges in long-term iodine storage requirements for adsorbent materials. Recently, many LDH-type materials (such as NiTi-LDH and MgAl-LDH) have shown high iodine adsorption efficiency based on chemical adsorption. However, the chemical adsorption of iodine is still limited in an aqueous environment.[4,9] Chemical adsorption combined with physical adsorption on NiTi-S_x-LDH in a humid air environment was considered to be an effective method for iodine adsorption for short-term storage.[36]

Table 1 The basic reactions for the formation of iodine compounds, and the corresponding changes in the Gibbs free energy (ΔG) at 200 °C calculated using the HSC code.[35]

Reaction	ΔG (kcal)	Spontaneity
$Ag + 1/2I_2(g) = AgI$	−16.059	Spontaneous
$Bi + 1/2O_2(g) + 1/2I_2(g) = BiOI$	−52.428	Spontaneous
$Bi + 3/2I_2(g) = BiI_3$	−33.376	Spontaneous
$5Bi + 7/2O_2(g) + 1/2I_2(g) = Bi_5O_7I$	−274.993	Spontaneous
$5/2Bi_2O_3 + 1/2I_2(g) = Bi_5O_7I + 1/4O_2(g)$	−5.867	Spontaneous
$2Bi_2O_3 + 2I_2(g) = 4BiOI + O_2(g)$	5.588	Nonspontaneous
$Bi_2O_3 + 3I_2(g) = 2BiI_3 + 3/2O_2(g)$	40.898	Nonspontaneous

Herein, various LDHs compounds were synthesized and characterized, where different amounts of Bi were used to modify the chemical activate characteristics of the LDHs. The experiments used the strong chemical attractions between iodine and bismuth in ZnAl LDH modified by Bi absorbents. Accordingly, BiZnAl-LDH was applied for iodine adsorption and storage over long periods.

2. Materials and methods

2.1. Materials

Zinc nitrate ($Zn(NO_3)_2\cdot 6H_2O$), sodium hydroxide (NaOH), aluminum nitrate ($Al(NO_3)_3\cdot 9H_2O$), bismuth nitrate ($Bi(NO_3)_3\cdot 5H_2O$), sodium carbonate (Na_2CO_3), and nitric acid (HNO_3) were purchased from Aladdin (China). All chemicals were used as received no additional pretreatment or purification.

2.2. Preparation of ZnAl-LDH modified by Bi

The BiZnAl-LDH adsorbent used herein was prepared *via* a coprecipitation method, which was previously reported.[4] Zinc nitrate ($Zn(NO_3)_2\cdot 6H_2O$) and aluminum nitrate ($Al(NO_3)_3\cdot 9H_2O$) were each dissolved in 200 mL deionized water, bismuth nitrate ($Bi(NO_3)_3\cdot 5H_2O$) was dissolved in concentrated nitric acid solution before adding water, and mixtures with the Bi : Zn : Al molar ratios of 0.1 : 3 : 0.9 (B1), 0.2 : 3 : 0.8 (B2), 0.3 : 3 : 0.7 (B3) and 0.4 : 3 : 0.6 (B4) were prepared. Next, 200 mL of mixed solution containing NaOH (0.08 mol) and Na_2CO_3 (0.03 mol) were added to the above solution and vigorously stirred with a pH value of 9.5 at room temperature. Then, the obtained solution was transferred to a 500 mL two-necked flask and left to react for 24 h at 90 °C. The mixture was carefully filtered and washed with ultra-pure water several times and dried overnight at 60 °C to obtain a white colored powder. The product BiZnAl-LDH was then collected in a small glass bottle for further examination and iodine adsorption experiments.

2.3. Characterization techniques

In this experiment, pH was monitored an IS128 pH-meter. A NICOLET-IS5 FT-IR spectrometer was used to record Fourier-

transformed infrared spectra (FT-IR) in the wavenumber range of 400–4000 cm^{-1}. The morphology and energy dispersive X-ray spectroscopy (EDX) element mapping analysis of the samples were performed on a scanning electron microscope (SEM, JSM-7800F) and transmission electron microscope (HRTEM, TEM, JEOL-LEM-2100F). Powder X-ray diffraction (XRD, Rigaku Ultima IV) patterns were measured on a DMAX2500 in the 2θ range of 5–80° at a scanning rate of 8° per minute. X-ray photoelectron spectroscopy (XPS) was performed on a Thermo ESCALab 250XI. Thermogravimetric analysis (TGA) was performed using an STA 449 F3 thermogravimetry analyzer at a heating rate of 10 °C min^{-1} in the temperature range of 25 °C to 800 °C under an N_2 atmosphere.

2.4. Iodine adsorption experiments

To address the feasibility of different adsorbents, one of the key parameters is their iodine adsorption capacity. Accordingly, during the adsorption test, the adsorbed mass was measured to determine the above-mentioned iodine adsorption capacity. The iodine adsorption experiment was conducted according to the following procedure.[30] Firstly, an excess of 0.2 g I_2 was added the bottom of a serum bottle, and then, a small amount of around 100 mg of the adsorbent was placed in a conical disc plate on top of the bottle. The vial was closed and sealed, and the glass bottle was heated at 75 °C and ambient pressure. Thereafter (1–2 days), the bottle was cooled to room temperature, and the iodine capture was estimated by weighing. Afterwards, by considering the ratio between the reaction products, the mass of iodine existing in the adsorbed mass was calculated. It is worth mentioning that the adsorbed mass was obtained by taking the difference between the sample mass before the experiment was conducted and that obtained after. A digital balance with a specificity of 10^4 was employed. In addition, to calculate the adsorbed mass, the final mass was measured twice. The amount of iodine existing in the above-mentioned adsorbed mass was determined by means of analyzing the reaction products. Additionally, ZnAl-LDH and the commercial AgX reported by Mnasri *et al.* were used for comparison. The iodine adsorption experiments were repeated three times and the results of the average value (relative standard error less than 5%) were utilized for the data analysis. The iodine adsorption of BiZnAl-LDH was calculated using formulas (1), and a schematic of the experimental setup is shown in Fig. 1.

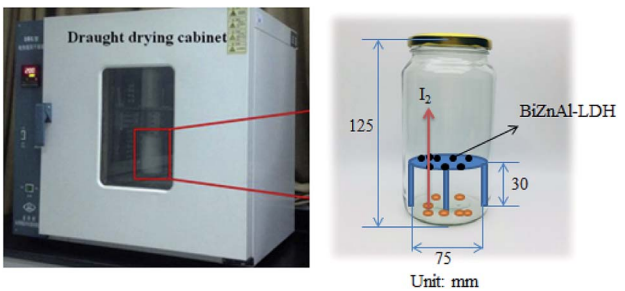

Fig. 1 Schematic of the device for the iodine adsorption experiments in static air.

$$Q\left(\frac{mg}{g}\right) = \frac{\Delta m}{m_s} \times 1000 \quad (1)$$

where Q (mg g^{-1}) is the iodine adsorption, m_s is the initial mass, and Δm is the mass gain of the sorbent.

3. Results and discussion

3.1. Characterization of BiZnAl-LDH

The FT-IR spectra of BiZnAl-LDH with various molar ratios of Bi/Zn/Al are shown in Fig. 2a. The small adsorption band at around 3769 cm^{-1} corresponds to M–OH. The broad band at around 3450 cm^{-1} is attributed to the interlayer molecules of water and the OH stretching mode of the layer hydroxyl group. The adsorption band at 2438 cm^{-1} is attributed to the carbonate ion interlayer of water molecule hydrogen bonds in BiZnAl-LDH. The bands for the C=O and H–O–H asymmetric stretching appear at 1745 and 1631 cm^{-1}, respectively. Compared with the CO_3^{2-} in $CaCO_3$ (1430 cm^{-1}), there was a significant shift in the absorption peak to 1349 cm^{-1}, indicating a change between CO_3^{2-} and H_2O through the hydrogen bond strength. The smaller bands in the range of 400–700 cm^{-1} are due to the LDH crystal lattice vibrations (Bi–O, Zn–O, and Al–O). The Bi–O stretching vibration, Zn–O and Al–O stretching vibration hare assigned to bands at 550 cm^{-1}, 436 cm^{-1} and 764 cm^{-1}, respectively.[31,37–39] The Al–O peaks in BiZnAl-LDH are weaker than that in ZnAl-LDH. In the same way as the atomic radius of Bi and Al, respectively, they are both of trivalent ions and are not

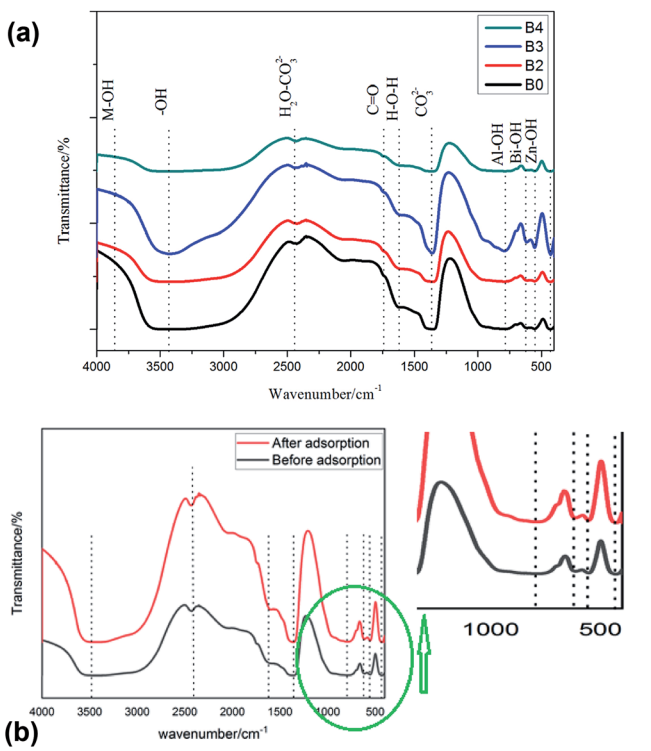

Fig. 2 (a) FTIR spectra of ZnAl-LDH (B0), $Bi_{0.2}ZnAl_{0.8}$-LDH (B2), $Bi_{0.3}ZnAl_{0.7}$-LDH (B3) and $Bi_{0.4}ZnAl_{0.6}$-LDH (B4). (b) FTIR spectra of BiZnAl-LDH (Bi/Zn/Al=0.4 : 3 : 0.6) before and after adsorption.

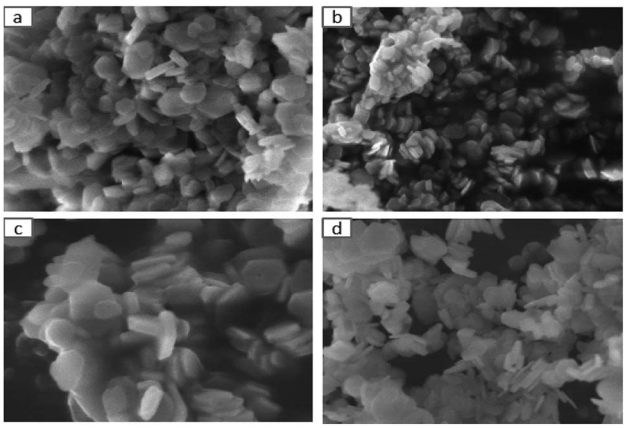

Fig. 3 SEM images of ZnAl-LDH (a), B2 (b), B3 (c) and B4 (d).

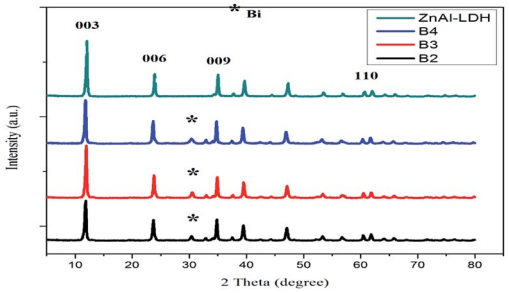

Fig. 5 XRD patterns of ZnAl-LDH, $Bi_{0.2}ZnAl_{0.8}$-LDH (B2), $Bi_{0.3}ZnAl_{0.7}$-LDH (B3) and $Bi_{0.4}ZnAl_{0.6}$-LDH (B4).

significant. The bismuth atoms can exchange with some of the aluminum atoms in the framework. However, the addition of Bi did not affect the crystal structure of the substrate, and the FT-IR spectrum of BiZnAl-LDH shows that Bi was effectively inserted into the ZnAl-LDH framework.

The FTIR spectrum in Fig. 2b after the sorption experiment shows that the I^- ion was present in BiZnAl-LDH-I. The strong bands in the range of 400–700 cm^{-1} are due to the LDH-iodine crystal lattice vibrations (BiI_3 and I_2–$ZnAl_2O_4$).

The characteristic SEM images of BiZnAl-LDH with different Bi/Zn/Al mole ratios and ZnAl-LDH are depicted in Fig. 3. It is obvious that all three BiZnAl-LDH samples exhibit a layered hexagonal structure similar to the typical structure of ZnAl-LDH with the layered hexagonal structure of $ZnAl_2O_4$.[39] The particle size and thickness of BiZnAl-LDH is about 200–300 nm and 40 nm, respectively. These results show that the lattice structure of the material was not destroyed after the addition of the appropriate amount of Bi.[40] Thus, based on the analysis above, BiZnAl-LDH was successfully synthesized through the co-precipitation method.[39]

Furthermore, the layered hexagonal structure of BiZnAl-LDH was studied *via* EDS, HRTEM, and TEM, as showed in Fig. 4. The TEM image in Fig. 4a and HRTEM image in Fig. 4b demonstrate that BiZnAl-LDH is mostly composed of different diameters of the hexagonal spherical particles. The typical HRTEM image, as presented in Fig. 4b, shows the layer structure of BiZnAl-LDH with *d*-spacings of 0.23 and 0.24 nm, corresponding to the different lattice planes of Bi and $ZnAl_2O_4$, respectively.[41–43] Fig. 4d shows the EDS mapping of a spherical particle, which was used to determine the composition of the hexagonal spherical particles of BiZnAl-LDH, confirming the results from the XPS analysis.

The XRD patterns of the samples are compared in Fig. 5. According to JCPDS: 48–1023, ZnAl-LDH shows extreme diffraction peaks located at $2\theta = 11.98°$, $23.84°$, $35.06°$ and

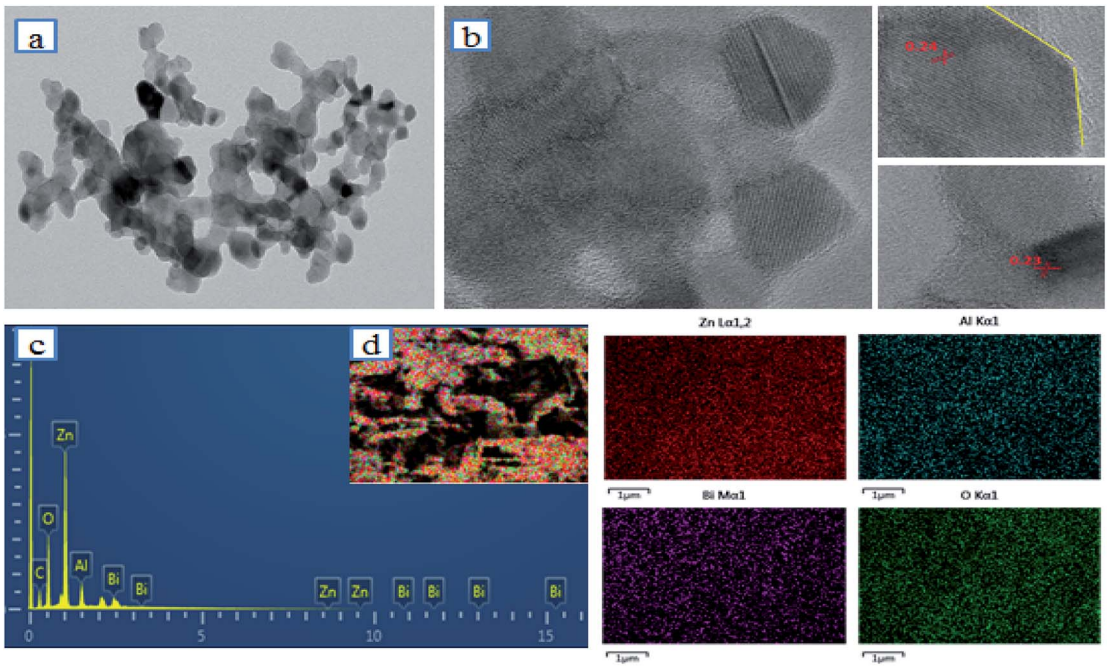

Fig. 4 (a) TEM image, (b) HRTEM image, (c) EDS results and (d) element mapping image of BiZnAl-LDH (Bi/Zn/Al=0.4 : 3 : 0.6).

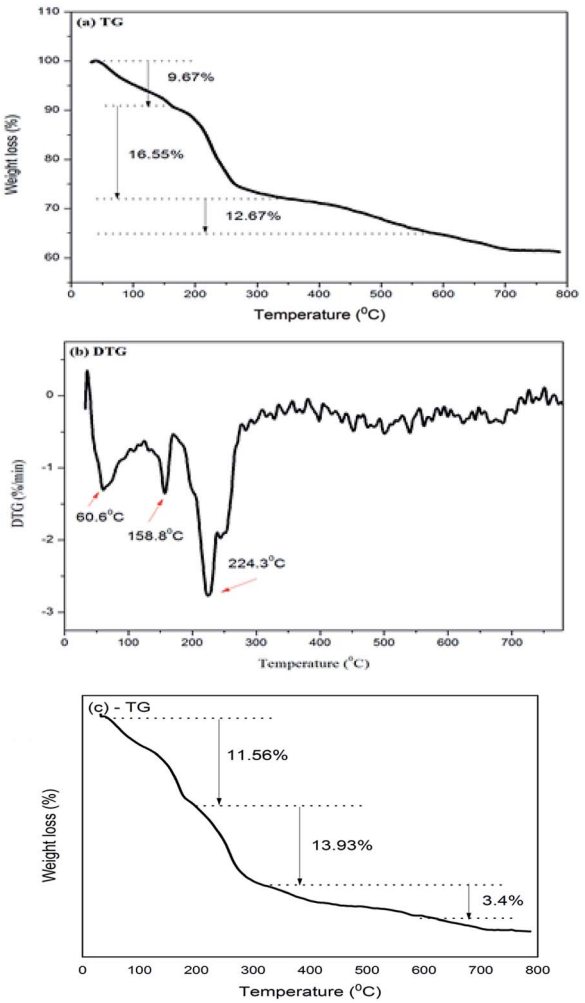

Fig. 6 TG-TDG curves of BiZnAl-LDH (Bi/Zn/Al=0.4 : 3 : 0.6) before (a) and (b), and after adsorption BiZnAl-LDH-I (c).

60.78°, corresponding to the (003), (006), (009), and (110) diffraction planes of ZnAl-LDH, respectively. BiZnAl-LDH exhibited similar diffraction peaks corresponding to the planes of ZnAl-LDH, and the total volume from the calculated LDH was greater than 80% of the reaction product. A broader peak indexed to Bi was discovered in BiZnAl-LDH due to the low percentage of Bi in BiZnAl-LDH at $2\theta = 30.46°$, which corresponds to the diffraction pattern of Bi (ICDD PDF No. 44-1246). As the molar ratio of Bi increased, the typical of XRD peaks of Bi become more intense, especially with the B4 sample, which showed the maximum intensity. Thus, based on the BiZnAl-LDH hexagonal structure reported in the literature (JCPDS No. 05-0669), the diffraction peak locations for ZnAl-LDH exhibited no change. All samples exhibited the characteristic diffraction peaks of the BiZnAl-LDH material, indicating that the layer structure of the LDH was not destroyed by the bismuth atoms.[39]

TG and DTG measurements were performed on the BiZnAl-LDH sample, and the results are shown in Fig. 6. According to the TG and DTG results for BiZnAl-LDH, three weight loss regions were observed. Specifically, the region between 40 °C to 200 °C (determined at 169.4 °C in DTG) is attributed to the loss of physically adsorbed water, between 200 °C to 600 °C (determined at 284.6 °C in DTG) is due to the loss of interlayer water dihydroxylation of the layered structure, and over 500 °C is due to the decomposition of carbonate, which is consistent with that for the previously reported $ZnAlCO_3$ LDH.[44] Similarly with LDH, the intrinsic form of dehydration at 40–200 °C (at 60.6 °C and 158.8 °C in DTG) and LDH layered structure of dihydroxylation distributed between 200 and 600 °C (especially the volume dropped sharply at 224.3 °C in DTG) can also be identified in the curves of BiZnAl-LDH.

3.2. Iodine adsorption studies

After the sample underwent complete adsorption with crystal iodine at 75 °C for 24 h, the color of the BiZnAl-LDH changed from white to dark grey (Fig. 7a and b, respectively). According to weight of the solid adsorbents before and after adsorption, the iodine adsorption capacity of BiZnAl-LDH was calculated to follow the order of B4 > B3 > B1 > B2 with values of 433, 374, 350, and 310 mg g^{-1}, respectively. This shows that the adsorption process of the synthetic materials is mainly chemical adsorption. Moreover, the pore volume and the corresponding pore diameter were calculated according to the Barrett–Joyner–Halenda model (BJH) for B1, B2, B3, and B4 to be 0.044, 0.035, 0.073 and 0.128 cm^3 g^{-1}, and 1.191, 1.322, 1.324 and 2.374 nm, respectively. Thus, the results of the experiment show the main role of Bi in BiZnAl-LDH. After adsorption, the EDS images and element distribution mapping of BiZnAl-LDH-I (Fig. 6c and d, respectively) still showed the layered hexagonal structure. There was a large amount of iodine in the samples, which preliminarily indicated the adsorption of iodine by BiZnAl-LDH, and the I_2 was reduced to I^{3-} between the intercalation layers and I_2 was chemically adsorbed on the layered BiZnAl-LDH.[35]

The functional groups and components of the material would have changed due to iodine adsorption. Therefore, we used XPS, XRD, and further characterization methods to further describe the reaction between BiZnAl-LDH and I_2. In Fig. 8, the XRD patterns of BiZnAl-LDH and BiZnAl-LDH-I show that the sorbents retained their typical structure after the iodine adsorption of hydrotalcite, and the characteristic absorption peaks of LDH still existed. The location of the peaks shifted and their intensity changed. In Fig. 8, the XRD pattern of BiZnAl-LDH-I after iodine adsorption demonstrates a change in the intensity of the peaks because of the nature of the hydrotalcite layers of the adsorbed iodine molecules.[45,46]

In Fig. 8, the XRD pattern of BiZnAl-LDH-I shows similar diffraction peaks to that of BiZnAl-LDH before iodine adsorption. Also, the characteristic adsorption peaks of LDH such as (003), (006), (009), and (110) still existed. However, the position and intensity of the peaks changed clearly after iodine adsorption. This shows that after iodine adsorption, the basal (d003) spacing of 0.24 nm in BiZnAl-LDH increased to 0.32 nm in BiZnAl-LDH-I. This indicates that the iodine exists in BiZnAl-LDH-I in the form of BiI_3, and also clearly shows that the atoms that compose the ZnAl-LDH crystal such as $ZnAl_2O_4$ participate in the iodine adsorption process. Also, the significant deviations in the intensity, and simultaneous shift in the

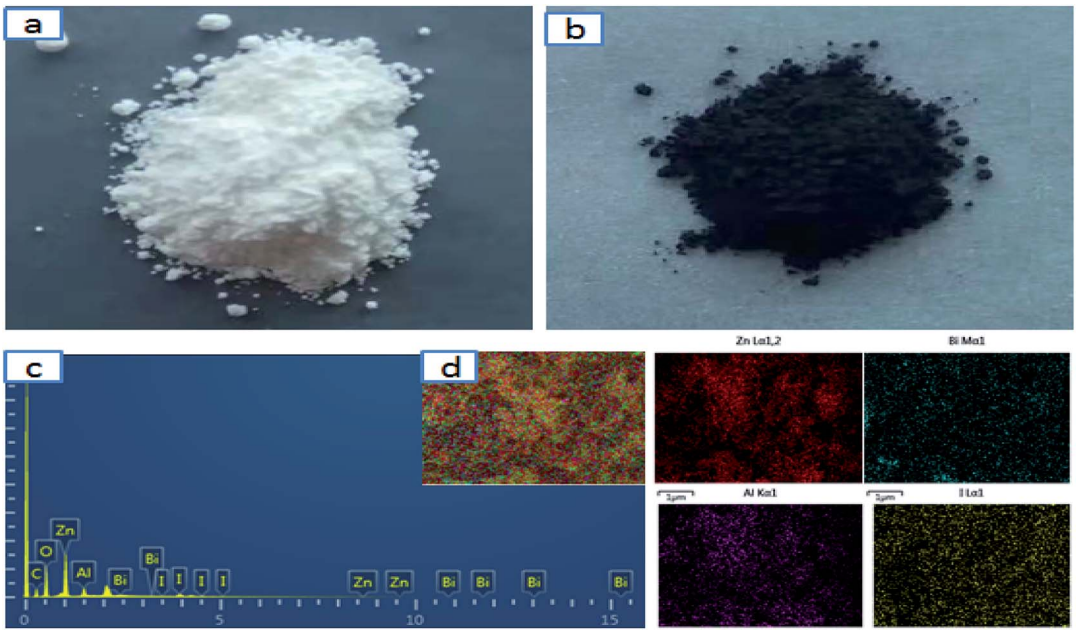

Fig. 7 (a) Optical image of BiZnAl-LDH, (b) optical image of BiZnAl-LDH-I, (c) EDS result and (d) element mapping image of BiZnAl-LDH-I.

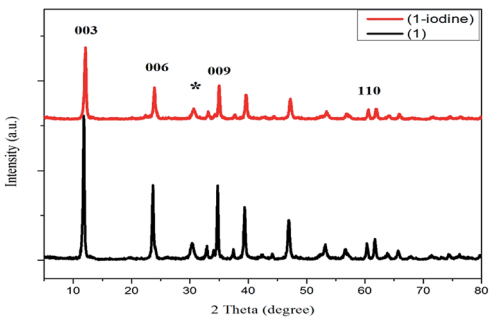

Fig. 8 XRD patterns of BiZnAl-LDH (1) and BiZnAl-LDH-I (1-iodine).

position of the peaks in the XRD pattern of BiZnAl-LDH-I are clearly demonstrated in the charge displacement produced in the XPS result in Fig. 9b for Bi 4f, Fig. 9c for Zn 2p and Fig. 9d for I 3d.

The survey XPS spectra (Fig. 9a) of before BiZnAl-LDH and after BiZnAl-LDH-I iodine adsorption show the presence of peaks for Zn 2p, Al 2p, Bi 4f, S 2p, and O 1s. After iodine adsorption, as shown in Fig. 9a, a new peak appeared at a binding energy of 618.6 eV for the BiZnAl-LDH-I sample, indicating that iodine was adsorbed. According to the XPS spectrum of I 3d (Fig. 9d), two peaks of I^{3-} $3d_{3/2}$ (at 630.1 eV) and I^{3-} $3d_{5/2}$ (at 618.6 eV) appeared.[47,48] Fig. 9b shows that the peaks of Bi $4f_{7/2}$ and Bi $4f_{5/2}$ in BiZnAl-LDH at 158.3 eV 163.6 eV transformed to the peaks of Bi $4f_{7/2}$ and Bi $4f_{5/2}$ in BiZnAl-LDH-I at 158.7 eV and 163.9 eV, respectively. However, the peaks of Zn $2p_{3/2}$ and Zn $2p_{1/2}$ also shifted from 1021.1 eV and 1044.2 eV in BiZnAl-LDH and to 1021.3 eV and 1044.4 eV for BiZnAl-LDH-I, respectively. In addition, a small volume of Al was also involved in iodine absorption process, when there is also small electronic shift from 73.7 eV to 73.9 eV. This can be explained by the electron adsorption of iodine atoms by the Bi atoms, Zn atoms and Al atoms. In the I 3d spectrum of BiZnAl-LDH-I, the peaks of I_2 at 618.6 eV and 630.1 eV shifted to 619.4 eV and 630.9 eV, respectively, for the molecule of BiI_3 containing iodine atoms, and 619.6 eV for iodine atom in ZnI_2.[30,49,50]

In Fig. 6c, the curve (TGA) of BiZnAl-LDH-I shows three mass loss region. The first mass loss in the range of 40 °C to 200 °C is mainly due to the elimination of some hydration water and physically adsorbed iodine.[36] The second mass loss (200–350 °C) is attributed to the further removal of dehydroxylated hydrotalcite. The third obvious mass loss (350–600 °C) is assigned to the removal of I^- in the metal iodide. Thus, according to the comparison of the TGA curves of BiZnAl-LDH and BiZnAl-LDH-I, it can be concluded that the adsorption process is mainly based on chemical adsorption.[4]

3.3. Iodine process

The mechanism for the iodine adsorption in the BiZnAl-LDH system is one of the key factors to consider during the experiment design process. This mechanism essentially consists of three steps. During the first step, essentially in the form of BiI_3, the BiZnAl-LDH composite captures iodine. This process is determined by the reaction described in expression (2) as follows,

$$3/2\ I_2 + Bi = BiI_3 \quad (2)$$

Fig. 10 shows the result of the physical adsorption during the second step of the aforementioned mechanism for the iodine adsorption, where a relatively small quantity of iodine exists in the form of I_2 in the BiZnAl-LDH compound. Finally, in the third step of the mechanism, a considerable quantity of iodine

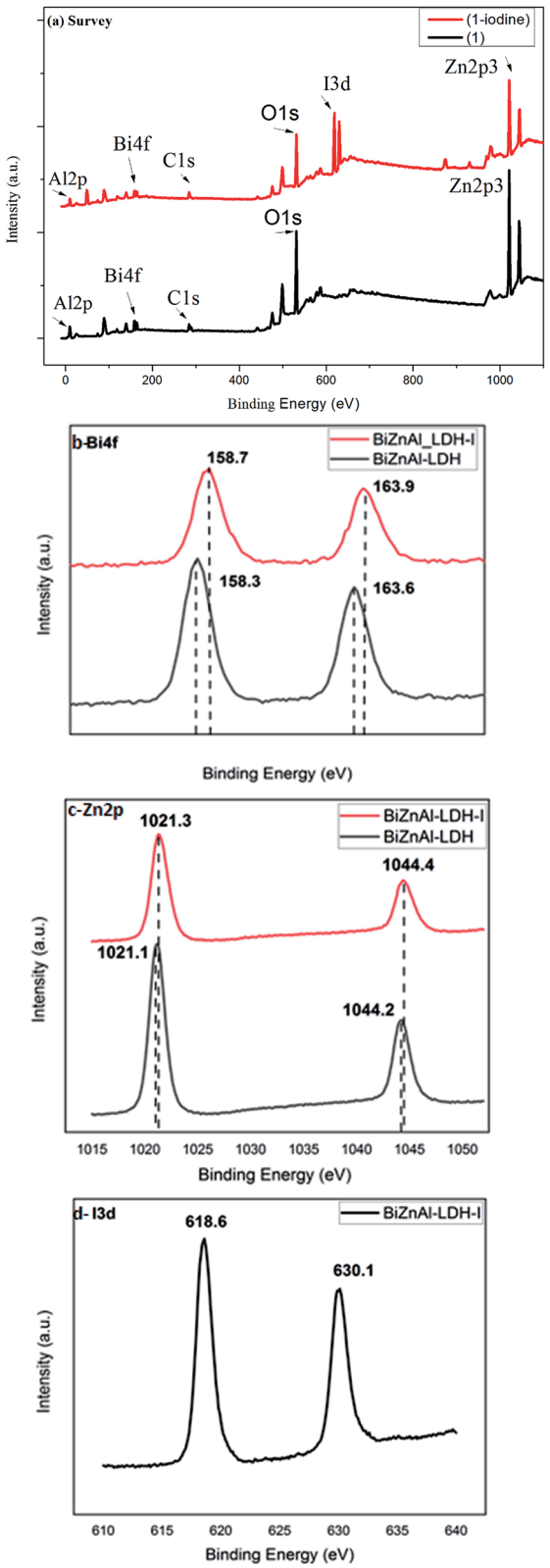

Fig. 9 (a) XPS survey spectra, (b) Bi 4f, (c) Zn 2p and (d) I 3d of BiZnAl-LDH (1) and BiZnAl-LDH-I (1-iodine).

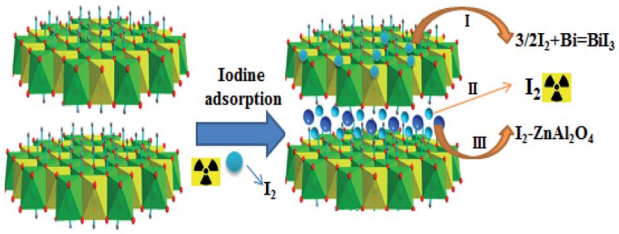

Fig. 10 Proposed mechanism of the iodine adsorption reaction on BiZnAl-LDH.

is captured due to $ZnAl_2O_4$, which is an expected result considering the chemical doping nature of the reaction involved in this third and final of the adsorption mechanism.

4. Conclusion

Herein, we reported the successful synthesis of BiZnAl-LDH through a co-precipitation method. The phase identity, optical response, and morphological structure of the hexagonal material were systematically characterized by FTIR, BET, SEM-EDS, XRD, XPS, TEM, HRTEM, and TG-DSC. In addition, the experimental procedures were carried out under the conditions of Bi/Al ratio of 0.4 : 0.6, for 24 h at 90 °C, and the highest adsorption capacity of the material was calculated to be about 433 (mg g^{-1}), which is approximately two times that of the commercial Ag-exchange zeolite X. Moreover, the surface area, pore volume, and average pore diameter of the as-synthesized material were 36.259 (m^2 g^{-1}), 0.128 (cm^3 g^{-1}), and 2.374 (nm), respectively. Furthermore, the BiZnAl-LDH material presented a hexagonal shape formed by ZnAl-LDH modified by Bi. Our results showed that iodine can be captured by mixing with BiZnAl-LDH through the reaction of bismuth, zinc, and doped $ZnAl_2O_4$. Moreover, our results showed that LDH-modified products of Bi can be used to adsorb iodine from fuel gas to replace the Ag-exchange zeolite X.

Author contributions

The manuscript was written through contributions of all authors. All authors have given approval to the final version of the manuscript.

Funding sources

This work was supported by the China Scholarship Council (2017GXZ019688).

Conflicts of interest

There are no conflicts to declare.

Acknowledgements

The authors acknowledge the valuable contributions of the Beijing Institute of Technology Analysis & Testing Center.

References

1 L. He, S. Liu, L. Chen, X. Dai, J. Li, M. Zhang, F. Ma, C. Zhang, Z. Yang, R. Zhou, Z. Chai and S. Wang, *Chem. Sci.*, 2019, **10**, 4293–4305.
2 J. Yu, X. Luo, B. Liu, J. Zhou, J. Feng, W. Zhu, S. Wang, Y. Zhang, X. Lin and P. Chen, *J. Mater. Chem. A*, 2018, **6**, 15359–15370.
3 J. Li, X. Dai, L. Zhu, C. Xu, D. Zhang, M. A. Silver, P. Li, L. Chen, Y. Li, D. Zuo, H. Zhang, C. Xiao, J. Chen, J. Diwu, O. K. Farha, T. E. Albrecht-Schmitt, Z. Chai and S. Wang, *Nat. Commun.*, 2018, **9**, 1–11.
4 G. Lin, L. Zhu, T. Duan, L. Zhang, B. Liu and J. Lei, *Chem. Eng. J.*, 2019, **378**, 122181.
5 Z. Ding, J. T. Kloprogge, R. L. Frost, G. Q. Lu and H. Y. Zhu, *J. Porous Mater.*, 2001, **8**, 273–293.
6 M. Takahashi, M. Takeda and Y. Ito, *Hyperfine Interact.*, 1994, **84**, 575–581.
7 P. Yi, A. Aldahan, V. Hansen, G. Possnert and X. L. Hou, *Environ. Sci. Technol.*, 2011, **45**, 903–909.
8 G. Fetter, E. Ramos, M. T. Olguin, P. Bosch, T. López and S. Bulbulian, *J. Radioanal. Nucl. Chem.*, 1997, **221**, 63–66.
9 F. L. Theiss, G. A. Ayoko and R. L. Frost, *Chem. Eng. J.*, 2016, **296**, 300–309.
10 J. Warchoł, P. Misaelides, R. Petrus and D. Zamboulis, *J. Hazard. Mater.*, 2006, **137**, 1410–1416.
11 A. E. Osmanlioglu, *J. Hazard. Mater.*, 2006, **137**, 332–335.
12 J. Zhou, S. Hao, L. Gao and Y. Zhang, *Ann. Nucl. Energy*, 2014, **72**, 237–241.
13 F. Yu, Y. Chen, Y. Wang, C. Liu and W. Ma, *Appl. Surf. Sci.*, 2018, **427**, 753–762.
14 I. Framework, D. F. Sava, M. A. Rodriguez, K. W. Chapman, P. J. Chupas, J. A. Greathouse, P. S. Crozier and T. M. Nenoff, *J. Am. Chem. Soc.*, 2011, 12398–12401.
15 D. Yang, S. Sarina, H. Zhu, H. Liu, Z. Zheng, M. Xie, S. V Smith and S. Komarneni, *Angew. Chem., Int. Ed.*, 2011, **50**, 10594–10598.
16 J. Liu, L. Chen, H. Cui, J. Zhang, L. Zhang and C. Y. Su, *Chem. Soc. Rev.*, 2014, **43**, 6011–6061.
17 T. D. Bennett, P. J. Saines, D. A. Keen, J. C. Tan and A. K. Cheetham, *Chem.–Eur. J.*, 2013, **19**, 7049–7055.
18 J. T. Hughes, D. F. Sava, T. M. Nenoff and A. Navrotsky, *J. Am. Chem. Soc.*, 2013, **135**, 16256–16259.
19 M. Sánchez-Polo, J. Rivera-Utrilla, E. Salhi and U. von Gunten, *Water Res.*, 2007, **41**, 1031–1037.
20 X. Zhang, P. Gu, X. Li and G. Zhang, *Chem. Eng. J.*, 2017, **322**, 129–139.
21 P. Mao, J. Jiang, Y. Pan, C. Duanmu, S. Chen, Y. Yang, S. Zhang and Y. Chen, *Materials*, 2018, **11**, 1–11.
22 C. M. Yang and K. Kaneko, *J. Colloid Interface Sci.*, 2002, **246**, 34–39.
23 V. Rives, *Mater. Chem. Phys.*, 2002, **75**, 19–25.
24 Y. Zhao, R. L. Frost and W. N. Martens, *J. Phys. Chem. C*, 2007, **111**, 16290–16299.
25 G. Mascolo and M. C. Mascolo, *Microporous Mesoporous Mater.*, 2015, **214**, 246–248.
26 J. L. Krumhansl and T. M. Nenoff, *Appl. Geochem.*, 2011, **26**, 57–64.
27 T. Nenoff, J. L. Krumhansl and A. Rajan, *Mater. Res. Soc. Symp. Proc.*, 2008, **1043**, 329–334.
28 L. Zhang, A. A. S. Gonçalves, B. Jiang and M. Jaroniec, *ChemSusChem*, 2018, **11**, 1486–1493.
29 J. H. Yang, Y. J. Cho, J. M. Shin and M. S. Yim, *J. Nucl. Mater.*, 2015, **465**, 556–564.
30 H. Zou, F. Yi, M. Song, X. Wang, L. Bian, W. Li, N. Pan and X. Jiang, *J. Hazard. Mater.*, 2019, **365**, 81–87.
31 H. Li, Q. Deng, J. Liu, W. Hou, N. Du, R. Zhang and X. Tao, *Catal. Sci. Technol.*, 2014, **4**, 1028–1037.
32 D. Sokol, M. Ivanov, A. N. Salak, R. Grigalaitis, J. Banys and A. Kareiva, *Mater. Sci.-Pol.*, 2019, **37**, 190–195.
33 A. Jaiswal and M. C. Chattopadhyaya, *Arabian J. Chem.*, 2017, **10**, S2457–S2463.
34 J. Long, Z. Yang, X. Zeng and J. Huang, *RSC Adv.*, 2016, **6**, 92896–92904.
35 J. Hwan, J. Myeong, J. Jin, G. Il and M. Sung, *J. Nucl. Mater.*, 2015, **457**, 1–8.
36 S. Ma, S. M. Islam, Y. Shim, Q. Gu, P. Wang, H. Li, G. Sun, X. Yang and M. G. Kanatzidis, *Chem. Mater.*, 2014, **26**, 7114–7123.
37 R. C. Zeng, X. T. Li, Z. G. Liu, F. Zhang, S. Q. Li and H. Z. Cui, *Front. Mater. Sci.*, 2015, **9**, 355–365.
38 C. Bi, J. Li, L. Peng and J. Zhang, *Biomed. Res.*, 2017, **28**, 2065–2069.
39 Z. Zhang, Z. Yang, J. Huang, Z. Feng and X. Xie, *Electrochim. Acta*, 2015, **155**, 61–68.
40 R. Wang, Z. Yang, B. Yang, T. Wang and Z. Chu, *J. Power Sources*, 2014, **251**, 344–350.
41 S. Sepulveda-Guzman, N. Elizondo-Villarreal, D. Ferrer, A. Torres-Castro, X. Gao, J. P. Zhou and M. Jose-Yacaman, *Nanotechnology*, 2007, **18**, 33.
42 L. Zou, F. Li, X. Xiang, D. G. Evans and X. Duan, *Chem. Mater.*, 2006, **18**, 5852–5859.
43 Y. Zhao, M. Wei, J. Lu, Z. L. Wang and X. Duan, *ACS Nano*, 2009, **3**, 4009–4016.
44 Z. Li, M. Chen, Q. Zhang, J. Qu, Z. Ai and Y. Li, *Appl. Clay Sci.*, 2017, **144**, 115–120.
45 N. Iyi, T. Matsumoto, Y. Kaneko and K. Kitamura, 2004, 2926–2932.
46 M. Bastianini, D. Costenaro, C. Bisio, L. Marchese, U. Costantino, R. Vivani and M. Nocchetti, *Inorg. Chem.*, 2012, **51**, 2560–2568.
47 K. Li, Y. Zhao, P. Zhang, C. He, J. Deng, S. Ding and W. Shi, *Appl. Surf. Sci.*, 2016, **390**, 412–421.
48 D. K. L. Harijan, V. Chandra, T. Yoon and K. S. Kim, *J. Hazard. Mater.*, 2018, **344**, 576–584.
49 D. Xu, D. Fan and W. Shen, *Nanoscale Res. Lett.*, 2013, **8**, 1–9.
50 F. Barka-Bouaifel, B. Sieber, N. Bezzi, J. Benner, P. Roussel, L. Boussekey, S. Szunerits and R. Boukherroub, *J. Mater. Chem.*, 2011, **21**, 10982–10989.